Polarimetric scattering from a two-dimensional improved sea fractal surface*

Liu Wei(刘 伟)†, Guo Li-Xin(郭立新), and Wu Zhen-Sen(吴振森)

School of Science, Xidian University, Xi'an 710071, *China*

(Received 3 August 2009; revised manuscript received 26 November 2009)

This paper studies the influence of wind parameters and fractal dimension from an improved two-dimensional sea fractal surface on the polarimetric scattering by using facet integration. A two-dimensional improved sea surface simulated is discretized into three matrices of sea surface facets including a height matrix and two slope matrices on orthogonal directions. Based on the Kirchhoff approximation, the polarimetric scattered field is derived in the Cartesian coordinate system by integration of three matrices mentioned above. Finally, the fully polarised radar cross section is numerically simulated and the dependence of the polarimetric scattering on the sea fractal surface, such as the wind speed, the wind direction, as well as the fractal dimension, is discussed in detail.

Keywords: polarimetric scattering, sea fractal surface, wind speed, wind direction
PACC: 4110H, 9210H

1. Introduction

The research of the sea surface scattering is widely applied to the area of the ocean remote sensing, target detection and identification, as well as the measurement of the oceanic environment and computer simulation.[1−6] Since the practical measurement of the sea surface scattering data requires an enormous cost and sea parameters are limited by the real sea condition, the simulation of sea echo data based on the rough surface electromagnetic scattering theory plays an important role in the investigation of the sea surface electromagnetic scattering.

As is well known, the first key work of the sea surface electromagnetic scattering is to establish an appropriate sea surface model. Currently, surface models in the electromagnetic scattering mainly include the fractal model and the spectrum model. A two-dimensional (2-D) fractal model of the sea surface proposed by Berizzi *et al.*[7] is a foundation of the subsequent research on the sea fractal surface scattering. Guo and Wang[8] proposed an improved 2-D sea fractal surface model with considering when the spatial wave number is less than the fundamental wave number. Franceschetti *et al.*[9] explored the use of the extended boundary condition method for the evaluation of scattering and emission from natural profiles modeled as a Weierstrass–Mandelbrot fractal function. Xie *et al.*[10] calculated the scattering fields of 2-D sea fractal surface with finite conductivity illuminated by ellipse polarisation wave in the Cartesian coordinate system within the Kirchhoff approximation (KA), but the integral kernel of the scattering fields neglected the effect of the sea surface slope. Similar to the influence of the height profile on the surface scattering, slopes in sea surface also affect the polarimetric scattering. Elfouhaily and Guerin[11] pioneered the concept of asymptotic solutions dynamically driven by surface properties, more specifically local curvature characteristics. To the authors' knowledge, few papers studied the relation between the slope distribution of sea surface and the polarimetric scattering coefficient. This paper presents a new expression of the polarimetric scattering coefficient based on the KA and matrix calculation.

The paper is organised as follows: the 2-D improved sea fractal model is introduced in Section 2, and the polarimetric scattered field is derived in the Cartesian coordinate system by using facet integration in Section 3. Then, differences of polarimetric scattering radar cross section (RCS) in different wind speeds, wind directions, fractal dimensions and incident angles are discussed in Section 4. Finally, Section 5 ends with the conclusions of the paper and proposed the further investigation in this topic.

*Project supported by the National Natural Science Foundation of China (Grant No. 60971067) and the Specialized Research Fund for the Doctoral Program of Higher Education of China (Grant No. 20070701010).
†Corresponding author. E-mail: liuwei@mail.xidian.edu.cn
© 2010 Chinese Physical Society and IOP Publishing Ltd

2. The 2-D improved sea fractal surface model

A 2-D improved sea fractal model is presented by Guo and Wang[8]:

$$\begin{aligned} & f(x,y,t) \\ = & \sigma\eta \sum_{m=0}^{N-1} a^{-(s-\xi)m} \sin\{K_0 a^m[(x+V_x t)\cos\beta_{1m} \\ & + (y+V_y t)\sin\beta_{1m}] - \Omega_{1m} t + \Phi_{1m}\} \\ & + \sigma\eta \sum_{n=0}^{N-1} b^{(s-3)n} \sin\{K_0 b^n[(x+V_x t)\cos\beta_{2n} \\ & + (y+V_y t)\sin\beta_{2n}] - \Omega_{2n} t + \Phi_{2n}\}, \end{aligned} \tag{1}$$

where σ is standard deviation, $\sigma = 0.0146u^2$, u is the wind speed measured at a 10 m height over the sea surface, η is normalised constant, $2 < s < 3$ is the fractal dimension, a represents the scale factor when spatial wavenumber is less than the fundamental frequency, b is the scale factor when spatial wavenumber is greater than fundamental frequency, K_0 is fundamental spatial wavenumber, V_x and V_y are radar motion velocity in x direction and y direction, respectively, Ω_{1m} and Ω_{2n} are angular frequencies, Φ_{1m} and Φ_{2n} are random wave phases which evenly distribute in $[-\pi, \pi]$, β_{1m} and β_{2n} are wave propagating directions which are functions of time in general, but for the sake of simplicity, they can be time-independent in a short time, so mean values of β_{1m} and β_{2n} could be equal to β_0, which is an angle between wind direction and x-axis, called the wind direction angle. Donelan direction function,[12] which is in good agreement with Chinese sea area, is one-order probability density function of $\psi_{1m} = \beta_{1m} - \beta_0$ and $\psi_{2n} = \beta_{2n} - \beta_0$,

$$P(K,\psi) = \frac{1}{2}\alpha \operatorname{sech}^2(\alpha\psi), \tag{2}$$

where

$$\begin{aligned} & \alpha = 2.61(K/K_0)^{1.3}, && 0.65 \le K/K_0 \le 0.95, \\ & \alpha = 2.28(K/K_0)^{-1.3}, && 0.95 < K/K_0 < 1.6, \\ & \alpha = 1.24, && \text{else} \quad K/K_0. \end{aligned} \tag{3}$$

3. Polarised scattering formulation

Scattering geometry and the local coordinate system of a 2-D sea surface is shown in Fig. 1, where θ_1 is an incident angle, θ_2 a scattering angle, θ_3 a relative azimuth to spatial position. Orthogonal coordinate systems of the incident field and the scattered field are defined as $(\hat{\boldsymbol{v}}_\mathrm{i}, \hat{\boldsymbol{h}}_\mathrm{i}, \hat{\boldsymbol{k}}_\mathrm{i})$ and $(\hat{\boldsymbol{v}}_\mathrm{s}, \hat{\boldsymbol{h}}_\mathrm{s}, \hat{\boldsymbol{k}}_\mathrm{s})$, respectively, and they can be expressed in the Cartesian coordinate system as

$$\begin{Bmatrix} \hat{\boldsymbol{k}}_\mathrm{i} \\ \hat{\boldsymbol{h}}_\mathrm{i} \\ \hat{\boldsymbol{v}}_\mathrm{i} \end{Bmatrix} = \begin{bmatrix} \sin\theta_1 & 0 & -\cos\theta_1 \\ 0 & 1 & 0 \\ -\cos\theta_1 & 0 & -\sin\theta_1 \end{bmatrix} \begin{Bmatrix} \hat{\boldsymbol{x}} \\ \hat{\boldsymbol{y}} \\ \hat{\boldsymbol{z}} \end{Bmatrix}, \tag{4}$$

$$\begin{Bmatrix} \hat{\boldsymbol{k}}_\mathrm{s} \\ \hat{\boldsymbol{h}}_\mathrm{s} \\ \hat{\boldsymbol{v}}_\mathrm{s} \end{Bmatrix} = \begin{bmatrix} \sin\theta_2\cos\theta_3 & \sin\theta_2\sin\theta_3 & \cos\theta_2 \\ -\sin\theta_3 & \cos\theta_3 & 0 \\ \cos\theta_2\cos\theta_3 & \cos\theta_2\sin\theta_3 & -\sin\theta_2 \end{bmatrix} \begin{Bmatrix} \hat{\boldsymbol{x}} \\ \hat{\boldsymbol{y}} \\ \hat{\boldsymbol{z}} \end{Bmatrix}, \tag{5}$$

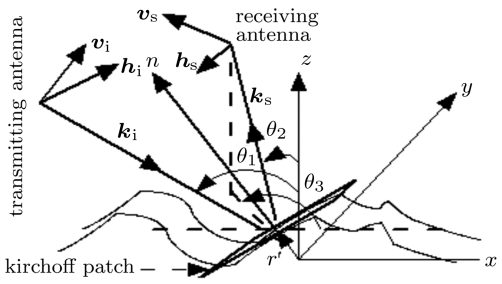


Fig. 1. Scattering geometry and local coordinate system.

The incident electric field is expressed as a vector sum of the horizontally polarised and vertically polarised electric field, i.e.,

$$\begin{aligned} \boldsymbol{E}_\mathrm{i}(\boldsymbol{r}) &= \boldsymbol{E}_\mathrm{i}^\mathrm{h} + \boldsymbol{E}_\mathrm{i}^\mathrm{v} \\ &= E_{01}\hat{\boldsymbol{h}}_\mathrm{i}\,\mathrm{e}_\mathrm{i}^{\mathrm{i}\boldsymbol{k}\cdot\boldsymbol{r}} + E_{02}\hat{\boldsymbol{v}}_\mathrm{i}\,\mathrm{e}^{\mathrm{i}(\boldsymbol{k}_\mathrm{i}\cdot\boldsymbol{r}+\gamma)}, \end{aligned} \tag{6}$$

where $\boldsymbol{k}_\mathrm{i}$ is a wavenumber vector of the incident wave, γ is a phase delay of $\boldsymbol{E}_\mathrm{i}^\mathrm{v}$ component to $\boldsymbol{E}_\mathrm{i}^\mathrm{h}$ component, E_{01} and E_{02} are the amplitude of horizontally polarised and vertically polarised electric field, respectively.

The illuminated sea fractal surface could be seen as a height matrix $\boldsymbol{Z}$ whose element $f'_{m,n}$ is the fractal surface height of a point $\boldsymbol{r'}_{m,n} = (x'_m, y'_n, f'_{m,n})$. The $\hat{\boldsymbol{n}}_{m,n}$ is described as a normal unit vector at a point $\boldsymbol{r'}_{m,n}$, i.e.,

$$\hat{\boldsymbol{n}}_{m,n} = \frac{-\alpha_{m,n}\hat{\boldsymbol{x}} - \beta_{m,n}\hat{\boldsymbol{y}} + \hat{\boldsymbol{z}}}{\sqrt{1+\alpha_{m,n}^2+\beta_{m,n}^2}}, \tag{7}$$

where $\alpha_{m,n}$ and $\beta_{m,n}$ are the slopes of the point $\boldsymbol{r}_{m,n}$ on the x and y directions, respectively. The subscripts

m and n which indicate the row and the column of the elements will be omitted in the following.

Meanwhile, a local orthogonal coordinate system of the point $\boldsymbol{r}'$ is defined as $(\hat{\boldsymbol{p}}_{\rm i}, \hat{\boldsymbol{q}}_{\rm i}, \hat{\boldsymbol{k}}_{\rm i})$, and $\hat{\boldsymbol{q}}_{\rm i} = \left(\hat{\boldsymbol{k}}_{\rm i} \times \hat{\boldsymbol{n}}\right) / \left|\hat{\boldsymbol{k}}_{\rm i} \times \hat{\boldsymbol{n}}\right|$, $\hat{\boldsymbol{p}}_{\rm i} = \hat{\boldsymbol{q}}_{\rm i} \times \hat{\boldsymbol{k}}_{\rm i}$, that is to say, $\hat{\boldsymbol{q}}_{\rm i}$ and $\hat{\boldsymbol{p}}_{\rm i}$ are the horizontally polarised and vertically polarised unit vector at the point $\boldsymbol{r}'$, respectively, which are given by

$$\begin{Bmatrix} \hat{\boldsymbol{q}}_{\rm i} \\ \hat{\boldsymbol{p}}_{\rm i} \end{Bmatrix} = \frac{1}{\sqrt{D}} \begin{bmatrix} (\alpha\cos\theta_1 - \sin\theta_1) & \beta \\ -\beta & (\alpha\cos\theta_1 - \sin\theta_1) \end{bmatrix} \times \begin{Bmatrix} \hat{\boldsymbol{h}}_{\rm i} \\ \hat{\boldsymbol{v}}_{\rm i} \end{Bmatrix}, \tag{8}$$

where $D = \beta^2 + (\alpha\cos\theta_1 - \sin\theta_1)^2$.

A horizontal component and a vertical component of the incident wave in the local orthogonal coordinate system are presented from Eqs. (6) and (8)

$$\begin{aligned} \boldsymbol{E}_{\rm i}^{\rm q} &= \frac{(\alpha\cos\theta_1 - \sin\theta_1)\, E_{01} + \beta E_{02}\, {\rm e}^{{\rm i}\gamma}}{\sqrt{D}}\, {\rm e}^{{\rm i}\boldsymbol{k}_{\rm i}\cdot\boldsymbol{r}} \boldsymbol{q}_{\rm i} \\ &= \left(E_{\rm hq} + E_{\rm vq}\, {\rm e}^{{\rm i}\gamma}\right) {\rm e}^{{\rm i}\boldsymbol{k}_{\rm i}\cdot\boldsymbol{r}} \boldsymbol{q}_{\rm i}, \end{aligned} \tag{9}$$

$$\begin{aligned} \boldsymbol{E}_{\rm i}^{\rm p} &= \frac{-\beta E_{01} + (\alpha\cos\theta_1 - \sin\theta_1)\, E_{02}\, {\rm e}^{{\rm i}\gamma}}{\sqrt{D}}\, {\rm e}^{{\rm i}\boldsymbol{k}_{\rm i}\cdot\boldsymbol{r}} \boldsymbol{p}_{\rm i} \\ &= \left(E_{\rm hq} + E_{\rm vp}\, {\rm e}^{{\rm i}\gamma}\right) {\rm e}^{{\rm i}\boldsymbol{k}_{\rm i}\cdot\boldsymbol{r}} \boldsymbol{p}_{\rm i}. \end{aligned} \tag{10}$$

The tangent plane of the point is regarded as an infinite plane, the reflected field for the horizontal component of the incident electric field can be given by

$$\boldsymbol{E}_{\rm r}^{\rm q} = R_{\rm h} \left(E_{\rm hq} + E_{\rm vq}\, {\rm e}^{{\rm i}\gamma}\right) {\rm e}^{{\rm i}\boldsymbol{k}_{\rm i}\cdot\boldsymbol{r}} \boldsymbol{q}_{\rm i}, \tag{11}$$

where $R_{\rm h}$ is the Fresnel reflection coefficient for $\boldsymbol{q}_{\rm i}$ polarisation, and is given by

$$R_{\rm h} = \frac{\cos\theta_{\rm l_i} - \sqrt{\varepsilon_{\rm r} - \sin^2\theta_{\rm l_i}}}{\cos\theta_{\rm l_i} + \sqrt{\varepsilon_{\rm r} - \sin^2\theta_{\rm l_i}}}, \tag{12}$$

where $\varepsilon_{\rm r}$ is the relative complex dielectric constant of sea water, $\theta_{\rm l_i}$ denotes the incident angle in the local coordinate system,

$$\cos\theta_{\rm l_i} = -\hat{\boldsymbol{n}} \cdot \hat{\boldsymbol{k}}_{\rm i} = \left(\frac{\alpha\sin\theta_1 + \cos\theta_1}{\sqrt{1 + \alpha^2 + \beta^2}}\right). \tag{13}$$

Then, the magnetic field corresponding to $\boldsymbol{E}_{\rm i}^{\rm q}$ and $\boldsymbol{E}_{\rm r}^{\rm q}$ can be expressed as

$$\boldsymbol{H}_{\rm i}^{\rm q} = \frac{1}{\eta} \hat{\boldsymbol{k}}_{\rm i} \times \left(E_{\rm hq} + E_{\rm vq}\, {\rm e}^{{\rm i}\gamma}\right) {\rm e}^{{\rm i}\boldsymbol{k}_{\rm i}\cdot\boldsymbol{r}} \boldsymbol{q}_{\rm i}, \tag{14}$$

$$\boldsymbol{H}_{\rm r}^{\rm q} = \frac{1}{\eta} \hat{\boldsymbol{k}}_{\rm r} \times \left(E_{\rm hq} + E_{\rm vq}\, {\rm e}^{{\rm i}\gamma}\right) R_{\rm h}\, {\rm e}^{{\rm i}\boldsymbol{k}_{\rm i}\cdot\boldsymbol{r}} \boldsymbol{q}_{\rm i}, \tag{15}$$

where local reflected wavenumber vector $\boldsymbol{k}_{\rm r} = \boldsymbol{k}_{\rm i} - 2\hat{\boldsymbol{n}}(\hat{\boldsymbol{n}} \cdot \boldsymbol{k}_{\rm i})$, the wave impedance $\eta = \sqrt{\mu_0/\varepsilon_0}$.

Similarly, an incident magnetic field and a reflected magnetic field of the incident electric field's local vertical component are as follows:

$$\boldsymbol{H}_{\rm i}^{\rm p} = \frac{1}{\eta} \hat{\boldsymbol{k}}_{\rm i} \times \left(E_{\rm hp} + E_{\rm vp}\, {\rm e}^{{\rm i}\gamma}\right) {\rm e}^{{\rm i}\boldsymbol{k}_{\rm i}\cdot\boldsymbol{r}} \boldsymbol{p}_{\rm i}, \tag{16}$$

$$\boldsymbol{H}_{\rm r}^{\rm p} = \frac{1}{\eta} \hat{\boldsymbol{k}}_{\rm i} \times R_{\rm v} \left(E_{\rm hp} + E_{\rm vp}\, {\rm e}^{{\rm i}\gamma}\right) {\rm e}^{{\rm i}\boldsymbol{k}_{\rm i}\cdot\boldsymbol{r}} \boldsymbol{p}_{\rm i}, \tag{17}$$

where $R_{\rm v}$ is the Fresnel reflection coefficient for $\boldsymbol{p}_{\rm i}$ polarisation,

$$R_{\rm v} = \frac{\varepsilon_{\rm r}\cos\theta_{\rm l_i} - \sqrt{\varepsilon_{\rm r} - \sin^2\theta_{\rm l_i}}}{\varepsilon_{\rm r}\cos\theta_{\rm l_i} + \sqrt{\varepsilon_{\rm r} - \sin^2\theta_{\rm l_i}}}, \tag{18}$$

The reflected electric field with $\boldsymbol{p}_{\rm i}$ polarisation is

$$\boldsymbol{E}_{\rm r}^{\rm p} = \left[\hat{\boldsymbol{k}}_{\rm i} \times R_{\rm v} \left(E_{\rm hp} + E_{\rm vp}\, {\rm e}^{{\rm i}\gamma}\right) {\rm e}^{{\rm i}\boldsymbol{k}_{\rm i}\cdot\boldsymbol{r}} \hat{\boldsymbol{p}}_{\rm i}\right] \times \hat{\boldsymbol{k}}_{\rm r}. \tag{19}$$

Adding $\boldsymbol{p}_{\rm i}$ polarisation component to $\boldsymbol{q}_{\rm i}$ polarisation component, we obtain a tangent electric field and a tangent magnetic field as

$$\hat{n} \times \boldsymbol{E}(\boldsymbol{r}') = \begin{bmatrix} \left(E_{\rm hq} + E_{\rm vq}\, {\rm e}^{{\rm i}\gamma}\right)(1 + R_{\rm h})\,(\hat{\boldsymbol{n}} \times \hat{\boldsymbol{q}}_{\rm i}) \\ + \left(E_{\rm hp} + E_{\rm vp}\, {\rm e}^{{\rm i}\gamma}\right)(1 - R_{\rm v}) \left(\hat{\boldsymbol{n}} \cdot \hat{\boldsymbol{k}}_{\rm i}\right) \hat{\boldsymbol{q}}_{\rm i} \end{bmatrix} {\rm e}^{{\rm i}\boldsymbol{k}_{\rm i}\cdot\boldsymbol{r}}, \tag{20}$$

$$\hat{n} \times \boldsymbol{H}(\boldsymbol{r}') = \frac{1}{\eta} \begin{bmatrix} -\left(E_{\rm hq} + E_{\rm vq}\, {\rm e}^{{\rm i}\gamma}\right)(1 - R_{\rm h}) \left(\hat{\boldsymbol{n}} \cdot \hat{\boldsymbol{k}}_{\rm i}\right) \hat{\boldsymbol{q}}_{\rm i} \\ + \left(E_{\rm hp} + E_{\rm vp}\, {\rm e}^{{\rm i}\gamma}\right)(1 + R_{\rm v})\,(\hat{\boldsymbol{n}} \times \hat{\boldsymbol{q}}_{\rm i}) \end{bmatrix} {\rm e}^{{\rm i}\boldsymbol{k}_{\rm i}\cdot\boldsymbol{r}}. \tag{21}$$

Based on Huygens theory,[13] the scattered field in upper zone can be expressed as

$$\boldsymbol{E}_{\rm s}(\boldsymbol{r}) = \int_{S'} {\rm d}S' \{{\rm i}\omega\mu_0 \overline{\overline{\boldsymbol{G}}}(\boldsymbol{r}, \boldsymbol{r}') \cdot [\hat{\boldsymbol{n}} \times \boldsymbol{E}(\boldsymbol{r}')] + \nabla \times \overline{\overline{\boldsymbol{G}}}(\boldsymbol{r}, \boldsymbol{r}') \cdot [\hat{\boldsymbol{n}} \times \boldsymbol{E}(\boldsymbol{r}')]\}, \tag{22}$$

where S' is sea surface area,. If observation point is in far zone, dyadic Green function is simplified as

$$\overline{\overline{\boldsymbol{G}}}(\boldsymbol{r},\boldsymbol{r}') = \left[\overline{\overline{\boldsymbol{I}}} - \hat{\boldsymbol{k}}_{\rm s}\hat{\boldsymbol{k}}_{\rm s}\right] \frac{{\rm e}^{{\rm i}kr}}{4\pi r}\, {\rm e}^{-{\rm i}\boldsymbol{k}_{\rm s}\cdot\boldsymbol{r}'}, \tag{23}$$

where $|\boldsymbol{k}_{\rm i}| = |\boldsymbol{k}_{\rm s}| = k$.

Equation (22) can be written as follows by substituting Eq. (23):

$$\boldsymbol{E}_{\rm s}(\boldsymbol{r}) = \frac{{\rm i}k\,{\rm e}^{{\rm i}kr}}{4\pi r}\left[\overline{\overline{\boldsymbol{I}}} - \hat{\boldsymbol{k}}_{\rm s}\hat{\boldsymbol{k}}_{\rm s}\right]\cdot\iint_{A_0}{\rm d}x'\,{\rm d}y'\boldsymbol{F}(\alpha,\beta)\,{\rm e}^{{\rm i}\hat{\boldsymbol{k}}_{\rm d}\cdot\boldsymbol{r}'}, \tag{24}$$

where A_0 is the projection of S' on the x–y plane, $\boldsymbol{k}_{\rm d} = \boldsymbol{k}_{\rm i} - \boldsymbol{k}_{\rm s}$, and the kernel of the integral is given by

$$\boldsymbol{F}(\alpha,\beta) = (1+\alpha^2+\beta^2)^{\frac{1}{2}}\left\{\begin{array}{l}\left(E_{\rm hq} + E_{\rm vq}\,{\rm e}^{{\rm i}\gamma}\right)\left[-(\hat{\boldsymbol{n}}\cdot\hat{\boldsymbol{k}}_{\rm i})\hat{\boldsymbol{q}}_{\rm i}(1-R_{\rm h}) + (\hat{\boldsymbol{k}}_{\rm s}\times(\hat{\boldsymbol{n}}\times\hat{\boldsymbol{q}}_{\rm i}))(1+R_{\rm h})\right] \\ +\left(E_{\rm hp} + E_{\rm vp}\,{\rm e}^{{\rm i}\gamma}\right)\left[(\hat{\boldsymbol{n}}\times\hat{\boldsymbol{q}}_{\rm i})(1+R_{\rm v}) + (\hat{\boldsymbol{n}}\cdot\hat{\boldsymbol{k}}_{\rm i})(\hat{\boldsymbol{k}}_{\rm s}\times\hat{\boldsymbol{q}}_{\rm i})(1-R_{\rm v})\right]\end{array}\right\}, \tag{25}$$

In the Cartesian coordinate system, the above expression could be rewritten as

$$\boldsymbol{F}(\alpha,\beta) = \left[\left(E_{\rm hq} + E_{\rm vq}\,{\rm e}^{{\rm i}\gamma}\right)(g_1\hat{\boldsymbol{x}} + h_1\hat{\boldsymbol{y}} + m_1\hat{\boldsymbol{z}}) + \left(E_{\rm hp} + E_{\rm vp}\,{\rm e}^{{\rm i}\gamma}\right)(g_2\hat{\boldsymbol{x}} + h_2\hat{\boldsymbol{y}} + m_2\hat{\boldsymbol{z}})\right], \tag{26}$$

where the parameters in Eq. (26) is deduced as following,

$$g_1 = \frac{1}{\sqrt{D}}\left\{\begin{array}{l}-\beta\cos\theta_1\,(\alpha\sin\theta_1 + \cos\theta_1)\,(1-R_{\rm h}) \\ +\left[\sin\theta_2\sin\theta_3\left(\alpha\sin\theta_1 - \left(\alpha^2+\beta^2\right)\cos\theta_1\right) + \cos\theta_2\,(\beta\cos\theta_1 + \alpha\beta\sin\theta_1)\right](1+R_{\rm h})\end{array}\right\}, \tag{27}$$

$$h_1 = \frac{1}{\sqrt{D}}\left\{\begin{array}{l}\left[(\alpha\sin\theta_1 + \cos\theta_1)\,(\alpha\cos\theta_1 - \sin\theta_1)\right](1-R_{\rm h}) + \left[\cos\theta_2\left(\left(\beta^2+1\right)\sin\theta_1 - \alpha\cos\theta_1\right)\right. \\ \left. -\sin\theta_2\cos\theta_3\left(\alpha\sin\theta_1 - \left(\alpha^2+\beta^2\right)\cos\theta_1\right)\right](1+R_{\rm h})\end{array}\right\}, \tag{28}$$

$$m_1 = \frac{1}{\sqrt{D}}\left\{\begin{array}{l}-\beta\sin\theta_1\,(\alpha\sin\theta_1 + \cos\theta_1)\,(1-R_{\rm h}) + [-\sin\theta_2\cos\theta_3\,(\beta\cos\theta_1 + \alpha\beta\sin\theta_1) \\ +\sin\theta_2\sin\theta_3\left(\alpha\cos\theta_1 - \left(\beta^2+1\right)\sin\theta_1\right)](1+R_{\rm h})\end{array}\right\}, \tag{29}$$

$$g_2 = \frac{1}{\sqrt{D}}\left\{\begin{array}{l}\left[\left(\beta^2+1\right)\sin\theta_1 - \alpha\cos\theta_1\right](1+R_{\rm v}) \\ +(\alpha\sin\theta_1 + \cos\theta_1)\,(\beta\sin\theta_1\sin\theta_2\sin\theta_3 + \alpha\cos\theta_1\cos\theta_2 - \sin\theta_1\cos\theta_2)\,(1-R_{\rm v})\end{array}\right\}, \tag{30}$$

$$h_2 = \frac{1}{\sqrt{D}}\left\{\begin{array}{l}(-\beta\cos\theta_1 - \alpha\beta\sin\theta_1)\,(1+R_{\rm v}) \\ +(\alpha\sin\theta_1 + \cos\theta_1)\,(\beta\cos\theta_1\cos\theta_2 - \beta\sin\theta_1\sin\theta_2\cos\theta_3)\,(1-R_{\rm v})\end{array}\right\}, \tag{31}$$

$$m_2 = \frac{1}{\sqrt{D}}\left\{\begin{array}{l}\left[\alpha\sin\theta_1 - \left(\alpha^2+\beta^2\right)\cos\theta_1\right](1+R_{\rm v}) \\ +(-\alpha\sin\theta_1 - \cos\theta_1)\,[\sin\theta_2\cos\theta_3(\alpha\cos\theta_1 - \sin\theta_1) + \beta\cos\theta_1\sin\theta_2\sin\theta_3]\,(1-R_{\rm v})\end{array}\right\}. \tag{32}$$

Substituting Eqs. (26)–(32) into the integral kernel of Eq. (24), we obtain

$$\boldsymbol{E}_{\rm s}(\boldsymbol{r}) = \frac{{\rm i}k\,{\rm e}^{{\rm i}kr}}{4\pi r}\left[\hat{\boldsymbol{v}}_{\rm s}\hat{\boldsymbol{v}}_{\rm s} + \hat{\boldsymbol{h}}_{\rm s}\hat{\boldsymbol{h}}_{\rm s}\right]\cdot\left[(G_1\hat{\boldsymbol{x}} + H_1\hat{\boldsymbol{y}} + M_1\hat{\boldsymbol{z}}) + (G_2\hat{\boldsymbol{x}} + H_2\hat{\boldsymbol{y}} + M_2\hat{\boldsymbol{z}})\,{\rm e}^{{\rm i}\gamma}\right], \tag{33}$$

where

$$G_1 = \int_{-X}^{X}\int_{-Y}^{Y}{\rm d}x'\,{\rm d}y'\,(E_{\rm hq}g_1 + E_{\rm hp}g_2)\,{\rm e}^{{\rm i}\hat{\boldsymbol{k}}_{\rm d}\cdot\boldsymbol{r}'}, \tag{34}$$

$$H_1 = \int_{-X}^{X}\int_{-Y}^{Y}{\rm d}x'\,{\rm d}y'\,(E_{\rm hq}h_1 + E_{\rm hp}h_2)\,{\rm e}^{{\rm i}\hat{\boldsymbol{k}}_{\rm d}\cdot\boldsymbol{r}'}, \tag{35}$$

$$M_1 = \int_{-X}^{X}\int_{-Y}^{Y}{\rm d}x'\,{\rm d}y'\,(E_{\rm hq}m_1 + E_{\rm hp}m_2)\,{\rm e}^{{\rm i}\hat{\boldsymbol{k}}_{\rm d}\cdot\boldsymbol{r}'}, \tag{36}$$

$$G_2 = \int_{-X}^{X}\int_{-Y}^{Y}{\rm d}x'\,{\rm d}y'\,(E_{\rm vq}g_1 + E_{\rm vp}g_2)\,{\rm e}^{{\rm i}\hat{\boldsymbol{k}}_{\rm d}\cdot\boldsymbol{r}'}, \tag{37}$$

$$H_2 = \int_{-X}^{X}\int_{-Y}^{Y}{\rm d}x'\,{\rm d}y'\,(E_{\rm vq}h_1 + E_{\rm vp}h_2)\,{\rm e}^{{\rm i}\hat{\boldsymbol{k}}_{\rm d}\cdot\boldsymbol{r}'}, \tag{38}$$

$$M_2 = \int_{-X}^{X}\int_{-Y}^{Y} \mathrm{d}x'\mathrm{d}y' \left(E_{\mathrm{vq}} m_1 + E_{\mathrm{vp}} m_2\right) \mathrm{e}^{\mathrm{i}\hat{\boldsymbol{k}}_{\mathrm{d}}\cdot\boldsymbol{r}'}, \tag{39}$$

$$\mathrm{e}^{\mathrm{i}\hat{\boldsymbol{k}}_{\mathrm{d}}\cdot\boldsymbol{r}'} = \exp\{\mathrm{i}[x'(\sin\theta_1 - \sin\theta_2\cos\theta_3) - y'\sin\theta_2\sin\theta_3 - z'(\cos\theta_1 + \cos\theta_2)]\}. \tag{40}$$

The total scattered field in Eq. (33) is decomposed into four following polarimetric components through the relationship between the orthogonal coordinate system of the scattered field and Cartesian coordinate system shown in Eq. (5), and each component can be expressed as

$$\boldsymbol{E}_{\mathrm{hh}}(\boldsymbol{r}) = \frac{\mathrm{i}k\,\mathrm{e}^{\mathrm{i}kr}}{4\pi r}\left[-\sin\theta_3 G_1 + \cos\theta_3 H_1\right]\hat{\boldsymbol{h}}_{\mathrm{s}}, \tag{41}$$

$$\boldsymbol{E}_{\mathrm{hv}}(\boldsymbol{r}) = \frac{\mathrm{i}k\,\mathrm{e}^{\mathrm{i}kr}}{4\pi r}\,\mathrm{e}^{\mathrm{i}\gamma}\left[-\sin\theta_3 G_2 + \cos\theta_3 H_2\right]\hat{\boldsymbol{h}}_{\mathrm{s}}, \tag{42}$$

$$\boldsymbol{E}_{\mathrm{vh}}(\boldsymbol{r}) = \frac{\mathrm{i}k\,\mathrm{e}^{\mathrm{i}kr}}{4\pi r}[\cos\theta_2\cos\theta_3 G_1 + \cos\theta_2\sin\theta_3 H_1 - \sin\theta_2 M_1]\hat{\boldsymbol{v}}_{\mathrm{s}}, \tag{43}$$

$$\boldsymbol{E}_{\mathrm{vv}}(\boldsymbol{r}) = \frac{\mathrm{i}k\,\mathrm{e}^{\mathrm{i}kr}}{4\pi r}\,\mathrm{e}^{\mathrm{i}\gamma}[\cos\theta_2\cos\theta_3 G_2 + \cos\theta_2\sin\theta_3 H_2 - \sin\theta_2 M_2]\hat{\boldsymbol{v}}_{\mathrm{s}}. \tag{44}$$

where the first and the second subscript of the polarimetric scatterd field denote the polarimetric direction of the scatterd field and the incident field, respectively.

Therefore, the Sinclair scattering matrix is obtained by

$$\boldsymbol{S} = \begin{bmatrix} s_{\mathrm{hh}} & s_{\mathrm{hv}} \\ s_{\mathrm{vh}} & s_{\mathrm{vv}} \end{bmatrix}, \tag{45}$$

where

$$s_{\mathrm{hh}} = \frac{\mathrm{i}k}{4\pi r E_{01}}\left[-\sin\theta_3 G_1 + \cos\theta_3 H_1\right], \tag{46}$$

$$s_{\mathrm{hv}} = \frac{\mathrm{i}k}{4\pi r E_{02}}\left[-\sin\theta_3 G_2 + \cos\theta_3 H_2\right], \tag{47}$$

$$s_{\mathrm{vh}} = \frac{\mathrm{i}k}{4\pi r E_{01}}[\cos\theta_2\cos\theta_3 G_1 + \cos\theta_2\sin\theta_3 H_1 - \sin\theta_2 M_1], \tag{48}$$

$$s_{\mathrm{vv}} = \frac{\mathrm{i}k}{4\pi r E_{02}}[\cos\theta_2\cos\theta_3 G_2 + \cos\theta_2\sin\theta_3 H_2 - \sin\theta_2 M_2]. \tag{49}$$

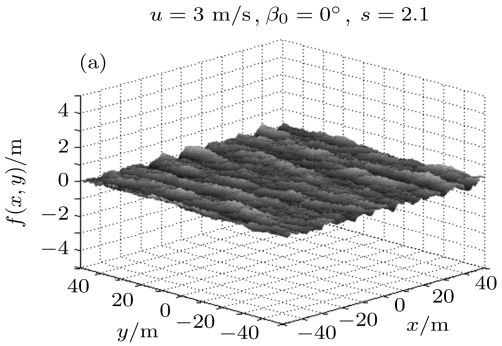
The expression for the fully polarised RCS is given by

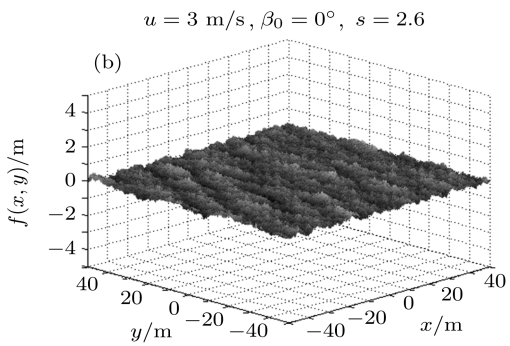
$$\sigma_{\mathrm{si}} = 4\pi r^2\left|s_{\mathrm{si}}\right|^2, \tag{50}$$

where $s = h_{\mathrm{s}}, v_{\mathrm{s}}$, $i = h_{\mathrm{i}}, v_{\mathrm{i}}$.

4. Numerical results and discussions

Let scaling factor $b = 1.105$, $a = 1/b$, the positive power ratio $\xi = 3.9$. Only the motionless radar platform is considered in this paper. Figure 2 shows four 2-D sea fractal surfaces with different parameters. As is depicted in Fig. 2, the fractal dimension is an important parameter to describe details of the sea surface, for a same wind speed, $u = 3$ m/s, Fig. 2(b) with $s = 2.6$ shows more capillary waves by comparing with the less fractal dimension, $s = 2.1$ in Fig. 2(a), and it is important to examine the fractal dimension because Bragg resonance may occur with the capillary waves for the shorter microwaves. The comparison of the surface profiles between Fig. 2(c) with $\beta_0 = 45°$ and Fig. 2(a) with $\beta_0 = 0°$, for the same condition $u = 3$ m/s, $s = 2.1$, shows different direction of the sea wave propagation, while the comparison of the surface height between Fig. 2(a) with $u = 3$ m/s and Fig. 2(d) with $u = 10$ m/s shows that the wind speed is a key factor to the wave height and sea wavelength.





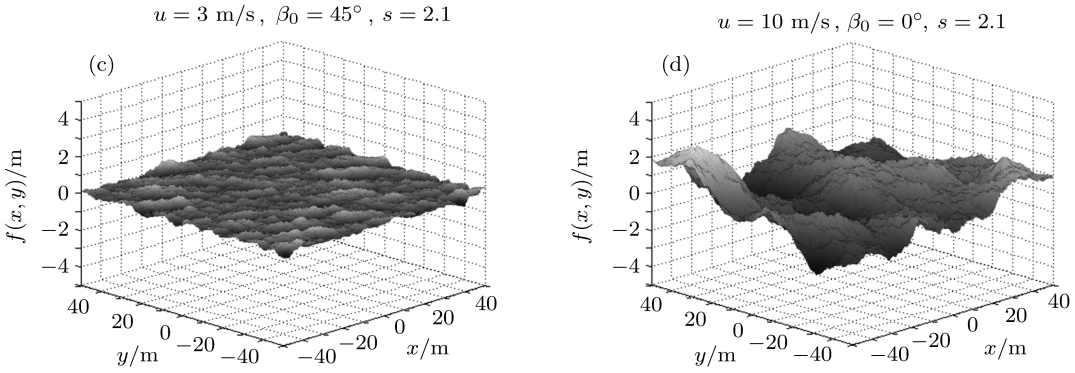


Fig. 2. The 2-D improved fractal sea model.

In order to investigate the performance of the proposed method, some simulations of fully polarised normalised RCS have been carried out with the incident frequency 1.3 GHz, the incident angle $\theta_1 = 20°$, and the azimuthal angle $\theta_3 = 0°$. The proposed method for simulating the normalised RCS has been tested under averaging 50 sea surface samples, and the fractal dimension of the surface is 2.1, the relative dielectric constant of sea water is chosen as 72.1–60.979i, the size of observed sea is 30 m×30 m.

Figure 3 illustrates the scattering pattern of RCS calculated by the method presented in the paper for the four polarisations with different wind speeds: 3 m/s, 10 m/s and the wind directions: 0°, 45°, 90°. From Figs. 3(a)–3(d), one can see that the value for the cross-polarised RCS is nearly 20 dB less than that for co-polarisation. The comparison of the scattering curve also shows the dependence of the polarimetric RCS on the wind speed and wind direction. As presented in Figs. 3(a) and 3(b), the effect of the wind direction to co-polarised (horizontal–horizontal polarization (HH) and vertical–vertical polarization (VV)) RCS is not obvious for $u = 3$ m/s, which may be caused by the fact that the height and wavelength of sea waves are so small relative to the observed sea size that the wind direction is not 'sensitive' to the co-polarised RCS. When the wind speed increases to 10 m/s, the influence of RCS on the wind direction becomes evident, and the value of the co-polarised RCS is visually large for upwind ($\beta_0 = 0°$) and small for crosswind ($\beta_0 = 90°$) over the whole scattering region. In addition, the co-polarised RCS of different wind directions are nearly equal in specular angle ($\theta_2 = 20°$) for the same wind speed. It is also observed that RCS of VV polarisation is less than that of HH polarisation at the large scattering angle due to the difference of the Fresnel reflection coefficient. Similarly, by comparison of the cross-polarised RCS at different wind speeds and wind directions, it is found that RCS of vertical–horizontal polarization (VH) polarisation is greater than that of horizontal–vertical polarization (HV) polarisation in general. Both of the cross-polarised RCS are equivalent in backscattering monostatic radar ($\theta_2 = -\theta_1$, $\theta_3 = 0°$) due to the reciprocity theorem. Consequently, RCS of VH polarisation shown in Fig. 3(d) has the minimum at $\theta_2 = -20°$. Similar to the co-polarised RCS, RCS of HV polarisation has a clear peak at specular scattering, and in particular RCS has maximum at $\beta_0 = 45°$ for the same wind speed. It is also seen that RCS of HV polarisation at $\beta_0 = 45°$ in a lower wind speed is still greater than that of upwind or crosswind in a higher wind speed, this phenomenon should not be really surprising, we attribute this behaviour to fact that the horizontal component of the vertical incident angle is the maximum in the local coordinate system when the wind direction angle is 45°.

To further explore the important scattering characteristic of the fractal surface model, in Fig. 4, we present the polarised RCS versus the scattering angle for different fractal dimensions and wind directions with the wind speed 3 m/s. It is readily found that the co-polarised RCS is not 'sensitive' to the variations of the fractal dimension and the wind direction, but to the cross-polarised RCS, the influence of the fractal dimension on the scattering curve is more obvious than that of the wind direction. Another point worth noting is that the cross-polarised RCS also has a peak value at $\beta_0 = 45°$, especially for the large fractal dimension. As a result, the effect of the cross-polarised RCS should be considered more emphatically in the retrieval of the fractal dimension and the wind direction.

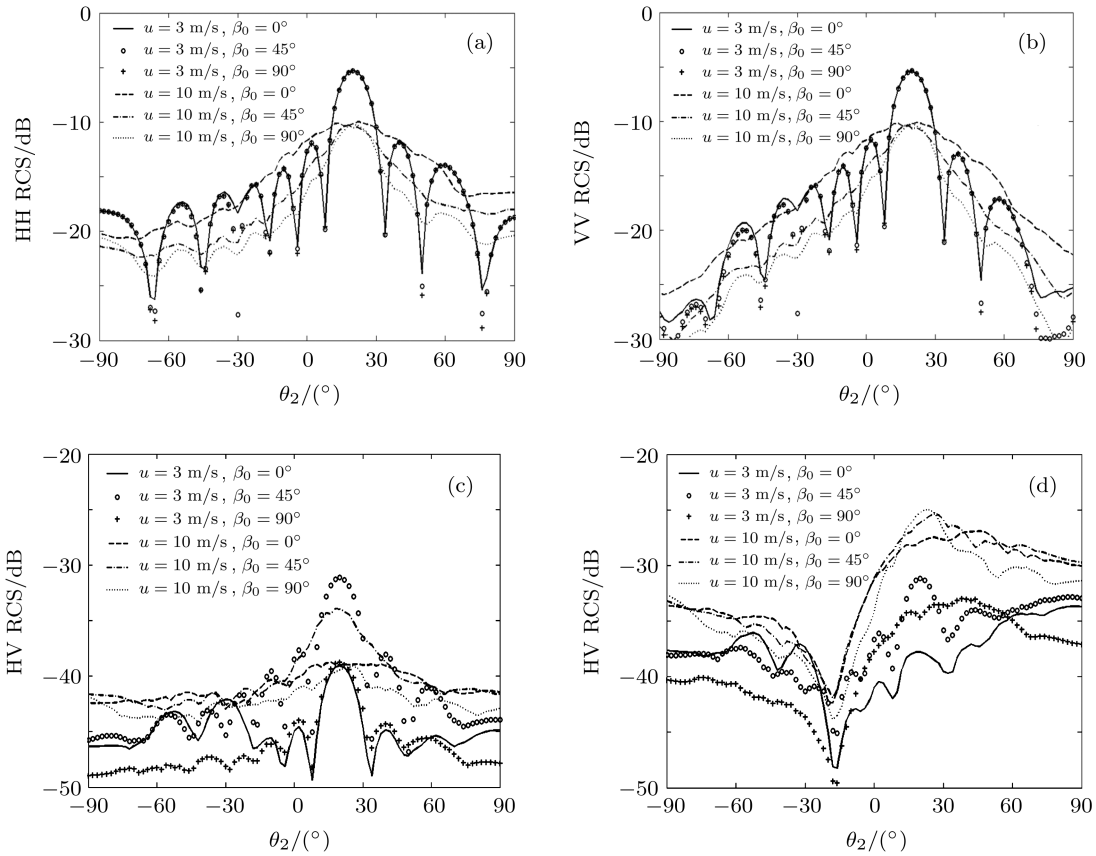


Fig. 3. Bistatic scattering in the incidence plane for different wind speeds and wind directions.

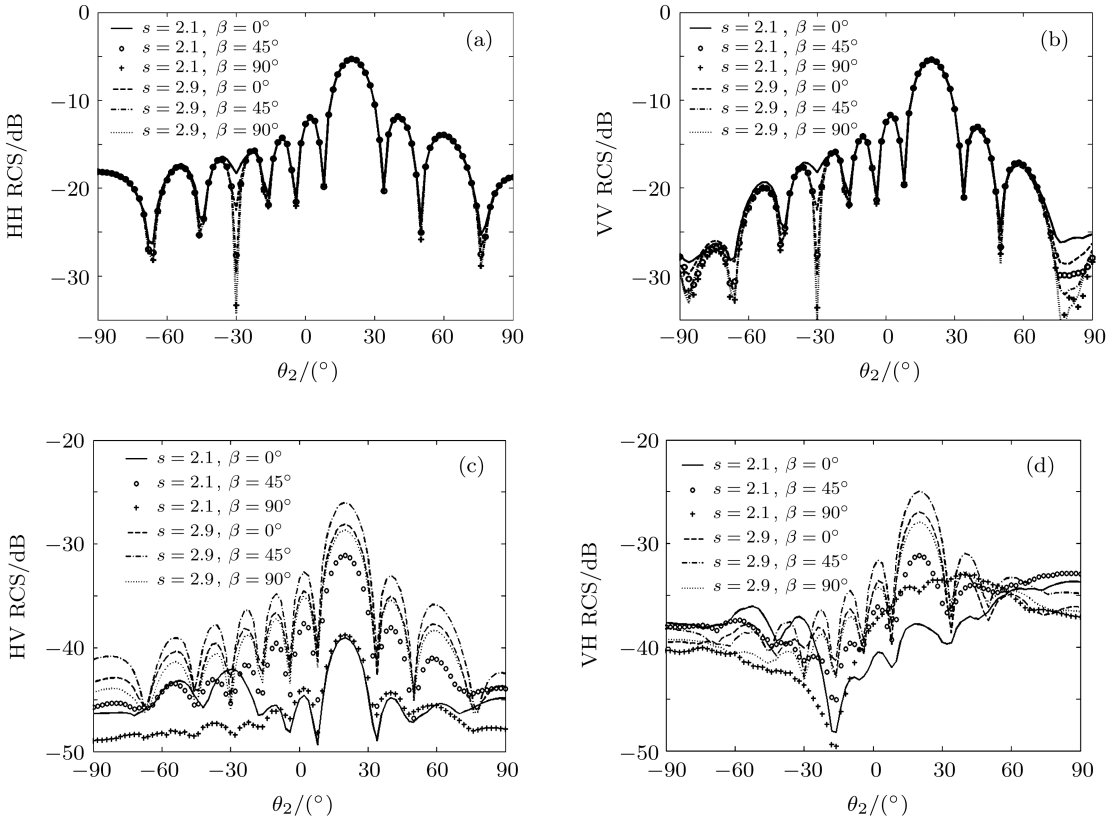


Fig. 4. Bistatic scattering in the incidence plane for different fractal dimensions and wind directions.

As seen previously, the difference of RCS between HH and VV polarisation is small, and based on the reciprocity theorem, RCS is equivalent for both HV and VH polarisation at monostatic radar where $\theta_1 = \theta_2$, $\theta_3 = 180°$, therefore, Fig. 5 only presents the monostatic RCS of HH and HV polarisation versus wind direction for different incident angles and wind speeds, the sea area is fixed at 100 m×100 m, and the other parameters are the same as those given in Fig. 3. Obviously, RCS in the co-polarisation and cross-polarisation at lower incident angle are greater than that at higher incident angle for the backscattering. Waves on the sea fractal surface could be regarded as low and long textures which are vertical to the wind direction when the area of observed sea is large and the wind speed is low. The cross-polarised RCS is sensitive to the direction of such small texture but the co-polarised RCS not. Therefore, as plotted in Fig. 5, RCS of HH polarisation remains basically unchanged, and HV polarisation has two peak values at 45° and 135°, when the wind speed is fixed at 3 m/s. At a larger wind speed, RCS of HH and HV polarisations are sensitive to the wind directions, the maximum appears in the upwind direction and the minimum in the crosswind direction. It should be pointed out that although the scattering behaviour is heavily influenced by the incident angle and the wind speed, the scattering curves show a good symmetry with respect to the cross wind direction ($\beta = 90°$), the primary reason for this is that the fractal sea model has no obvious difference between upwind and downwind. For large amplitude gravity and capillary-gravity waves, one effect of this curvature increase at the crest is that, as Kinsman described,[14] capillary waves come from just ahead of the crest on the forward and downwind face of the wave. Described in a fractal way, the dimension of the forward face should be greater than that of the backward face. But the actual anisotropic rough sea surface cannot be expressed exactly by the current fractal sea model, therefore, this disadvantage leads to the difficulty in dividing the RCS in the upwind and downwind direction by the presented polarimetric scattering model, thus, as a guideline for the next work, the polarimetric scattering from the actual sea surface in different wind directions with the multi-fractal model is advisable.

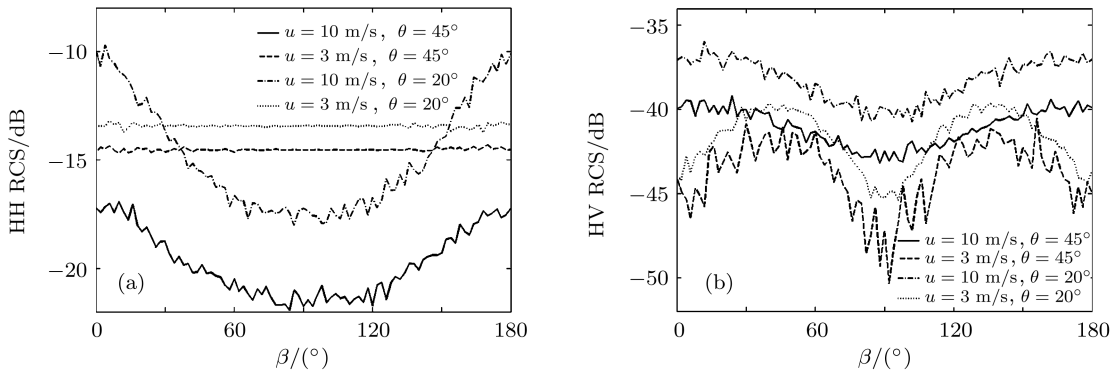


Fig. 5. Monostatic scattering versus the wind direction for different incident angle and wind speed.

5. Conclusion

We have proposed a new polarised scatter coefficient simulation of the sea rough surface. Starting from an improved fractal sea surface model and considering the local gradient of each facet into a KA kernel, we have deduced four expressions of polarised scattering coefficient by integrations on three orthogonal Cartesian coordinates. Numerical results present the influence of the wind speed, wind direction, fractal dimensions and incident angles on the polarimetric RCS from a 2-D improved fractal sea surface. The comparisons of the scattering pattern also show that the fully polarised RCS is heavily influenced by the wind speed, the incident angle and the fractal dimension, the cross-polarised RCS is more sensitive than co-polarised RCS to the wind direction and the fractal dimension, thus, the fractal dimension could be an important retrieval factor for wind direction at cross-polarisation. A possibility in the future work is to develop a new and reliable direct fractal sea surface scattering model with the considered multi-fractal to better describe the polarimetric scattering from the actual sea surface in different wind directions.

References

[1] Wang Y H, Guo L X and Wu Z J 2006 *Acta Phys. Sin.* **55** 5191 (in Chinese)

[2] Brelet Y and Bourlier C 2008 *Progress in Electromagnetics Research* **81** 413

[3] Wang R, Guo L X, Qin S T and Wu Z S 2008 *Acta Phys. Sin.* **57** 3473 (in Chinese)

[4] Li J, Guo L X, Zeng H and Han X B 2009 *Chin. Phys.* B **18** 2757

[5] Yang J L, Guo L X and Wan J W 2007 *Acta Phys. Sin.* **56** 2106 (in Chinese)

[6] Guo L X and Wu Z S 2004 *J. Electromagnetic Waves and Applications* **18** 1219

[7] Berizzi F, Mese E D and Pinelli G 1997 *Proceedings of Radar Systems* Edinburgh UK, 14–16 October, 1997 p189

[8] Guo L X and Wang Y H 2005 *Progress in Electromagnetics Research Symposium* Hangzhou China, 22-26 August, 2005 p23

[9] Franceschetti G, Iodice A, Riccio D and Ruello G 2005 *IEEE Trans. Geosci. Remote Sensing* **43** 1115

[10] Xie T, Li B H, Chen W J and He Y J 2004 *Geoscience and Remote Sensing Symposium* Alaska USA, 20–24 September, 2004 p2772

[11] Elfouhaily T and Guerin C A 2004 *Waves in Random Media* **14** R1

[12] Yu Y X and Liu S X 1995 *The Ocean Engineering* **13** 1 (in Chinese)

[13] Kong J A 1986 *Electromagnetic Wave Theory* (New York: Wiley)

[14] Kinsman B 1984 *Wind Waves: Their Generation and Propagation on the Ocean Surface* (New York: Dover Publications)